nature geoscience

ARTICLES

https://doi.org/10.1038/s41561-020-0599-9

Distinct formation history for deep-mantle domains reflected in geochemical differences

Luc S. Doucet[1]✉, Zheng-Xiang Li[1], Hamed Gamal El Dien[1,2], Amaury Pourteau[1], J. Brendan Murphy[1,3], William J. Collins[1], Nadine Mattielli[4], Hugo K. H. Olierook[5,6], Christopher J. Spencer[1,7] and Ross N. Mitchell[1,8]

The Earth's mantle is currently divided into the African and Pacific domains, separated by the circum-Pacific subduction girdle, and each domain features a large low shear-wave velocity province (LLSVP) in the lower mantle. However, it remains controversial as to whether the LLSVPs have been stationary through time or dynamic, changing in response to changes in global subduction geometry. Here we compile radiogenic isotope data on plume-induced basalts from ocean islands and oceanic plateaus above the two LLSVPs that show distinct lead, neodymium and strontium isotopic compositions for the two mantle domains. The African domain shows enrichment by subducted continental material during the assembly and breakup of the supercontinent Pangaea, whereas no such feature is found in the Pacific domain. This deep-mantle geochemical dichotomy reflects the different evolutionary histories of the two domains during the Rodinia and Pangaea supercontinent cycles and thus supports a dynamic relationship between plate tectonics and deep-mantle structures.

Present-day Earth's mantle structure is dominated by a degree-2 spherical harmonic featuring two equatorial and antipodal mantle domains bisected by a subduction girdle surrounding the Pacific Ocean. Each of the two antipodal African and Pacific mantle domains features a large low shear-wave velocity province (LLSVP) in the lower mantle. Although most mantle plumes are believed to have originated from the edges of the LLSVPs in the two mantle domains since at least ca. 200 million years ago (Ma)[1], we still know little about the nature and evolutionary histories of the two LLSVPs.

Opposing models exist regarding how and when the two LLSVPs formed. According to one model, they are quasi-stationary, long-lived through Earth history (4.0–2.0 billion years ago) and uninfluenced by plate tectonics[1,2]. By contrast, another model claims the LLSVPs are dynamic in their formation, evolution (including demise) and geographic locations and are linked to the assembly and breakup of supercontinents[3,4]. Palaeomagnetic data, mantle plume records during the last two supercontinent cycles and dynamic modelling results have been used to suggest that the antipodal LLSVPs are related to whole-mantle convection driven by plate motion[5,6], particularly by circum-supercontinent subduction[7]. As such, the shape and location of LLSVPs both in time and space are dynamically linked to the formation of supercontinents. It has been further speculated[3,7,8] that when the antipodal LLSVPs, whose locations are controlled by the subduction girdle surrounding the supercontinent, are positioned off the Equator, the centrifugal force of Earth's spin would bring them to the Equator through true polar wander, that is, wholesale rotation of the entire silicate Earth relative to the spin axis[9]. Such a strong coupling between the outer layer of the planet (tectonic plates) and deeper mantle domains is consistent with both continental and oceanic plume records over much of Earth history[10,11]. However, to test contrasting geodynamic models, it is fundamental to characterize and compare the geochemical compositions and evolutionary paths of the two mantle domains.

Radiogenic isotopes (lead (Pb), strontium (Sr) and neodymium (Nd)) and noble gas isotopes (for example, helium (He)) of basaltic lava flows originating from hotspots in the present-day oceans appear to be the best tools for evaluating any systematic compositional difference between the two mantle domains[12]. A first-order isotopic distinction can be made between mid-ocean-ridge basalts (MORBs) and hotspot basalts (or ocean island basalts (OIBs)), which are thought to tap reservoirs in the depleted upper mantle[13] and the more primitive lower mantle[14], respectively. While most MORBs are isotopically relatively uniform, OIBs show substantial diversity due to deep recycling of various subducted lithospheric components such as oceanic and continental lithospheric materials, including sediments[13].

Geographically, isotopic signatures from oceanic basalts have a purported hemispheric distinction[15], with OIBs from the Southern Hemisphere believed to have relatively higher $^{207}Pb/^{204}Pb$ and $^{208}Pb/^{204}Pb$ for a given $^{206}Pb/^{204}Pb$, higher $^{86}Sr/^{87}Sr$ and lower εNd compared with compositions from the Northern Hemispheric mantle[15]. Hart[16] defined the isotopic enrichment of southern basalts as the 'DUPAL anomaly' and ascribed it to a deep, ancient geochemical reservoir formed by preferential subduction in the Southern Hemisphere during the early stage of Earth differentiation above the core–mantle boundary[13,15]. However, the hypothesized latitudinal subdivision fails to explain the well-documented isotopic characteristics of basalts from the southwest Pacific region (that is, supposedly within the DUPAL domain) that are distinct from both south

[1]Earth Dynamics Research Group, TIGeR, School of Earth and Planetary Sciences, Curtin University, Perth, Western Australia, Australia. [2]Geology Department, Faculty of Science, Tanta University, Tanta, Egypt. [3]Department of Earth Sciences, St. Francis Xavier University, Antigonish, Nova Scotia, Canada. [4]Laboratoire G-Time, Université Libre de Bruxelles, ULB, Brussels, Belgium. [5]Timescales of Mineral Systems, Centre for Exploration Targeting—Curtin Node, Curtin University, Perth, Western Australia, Australia. [6]John de Laeter Centre, Curtin University, Perth, Western Australia, Australia. [7]Department of Geological Sciences and Geological Engineering, Queen's University, Kingston, Kingston, Ontario, Canada. [8]State Key Laboratory of Lithospheric Evolution, Institute of Geology and Geophysics, Chinese Academy of Sciences, Beijing, China. ✉e-mail: luc-serge.doucet@curtin.edu.au

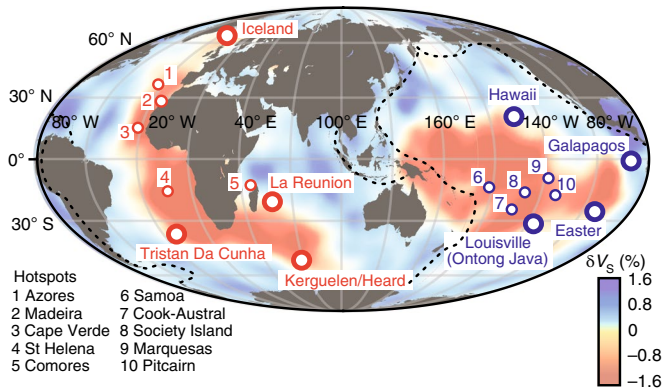

Fig. 1 | Global maps of the LLSVPs. Seismic shear-wave velocity anomalies (δV_s) are those of the mean S-wave tomography model s5mean[37]. Also shown are the major OIBs and OPBs, with large circles denoting plumes of deep origin[23] and small circles denoting plumes of shallower origin[23] (Extended Data Fig. 3). The map is centred on the Equator and 100th meridian, and each meridian is separated by 30°.

Atlantic and Indian Ocean basalts[17]. Hence, a South Pacific isotopic and thermal anomaly[17,18] has since been defined within the DUPAL anomaly. Over the past decades, attempts have been made to 'map' the DUPAL distribution to decipher the origin of geochemical heterogeneities in the lower mantle using extensive OIB data[13,18,19]. The isotopic heterogeneity of the mantle has therefore been well documented, but the processes that govern the spatial distribution of the lower mantle geochemical complexity remain cryptic.

Isotopic compositions of the two mantle domains

Combined geochemistry and geophysical imaging have established that the source materials of OIBs and oceanic plateau basalts (OPBs) do not necessarily all originate from the deep mantle[20]. Some hotspots are rooted at the edge of the LLSVPs[21,22], whereas others could have a shallower mantle source[23,24]. Hence, the radiogenic isotopic compositions of OPBs and OIBs worldwide might reflect both deep and shallow mantle signatures. To decipher the isotopic composition of deep-mantle materials, we compiled all available Pb, Sr, and Nd isotopic data (~6,000 samples; see Supplementary Data 1 and 2) on OPBs and OIBs, from which we distinguish the basalts from ocean islands and oceanic plateaus that have unambiguous deep-mantle source (~3,800 samples) following the criteria of Courtillot et al.[23]. This approach allowed us to mitigate the complicating effects of contamination by the continental crust, the continental lithosphere or the shallower upper convective mantle (Extended Data Figs. 1, 2 and 3). The primary criteria for recognizing basalts derived from the deep mantle are (1) flood basalts formed in the early history of the plume activity[23], (2) a long-lived hotspot track[23], (3) unambiguous tomographic evidence for a plume tail extending down to the core–mantle boundary[20,25] and (4) high $^3He/^4He$ ratios[24]. Among modern oceanic plateaus and hotspots associated with the African and Pacific mantle domains, six hotspots and two oceanic plateaus meet these criteria: Tristan da Cunha, La Reunion, Iceland and Kerguelen Plateau for the African mantle domain and Hawaii, Easter Islands, Galapagos Islands and Ontong Java for the Pacific mantle domain (Fig. 1 and Extended Data Fig. 3). Although some other flood basalts may also have been derived from deep plumes, Extended Data Fig. 1 illustrates that data from those basalts show more overlap between the two mantle domains. By using data from the selected deep-sourced plume basalts only (Fig. 2), we minimize the risk of inadvertently including basalts either derived from or contaminated by shallow-mantle sources.

The selected 3,869 sets of long-lived radiogenic isotopic data from basalts derived from the deep-mantle sources (Supplementary Data 1 and 2) demonstrate notable compositional differences between basalts derived from the African and Pacific mantle domains (Fig. 2). Most basalts sourced from the Pacific mantle domain have $^{87}Sr/^{86}Sr$ <0.705 and $^{207}Pb/^{204}Pb$ and $^{208}Pb/^{204}Pb$ similar to the Northern Hemisphere reference line (NHRL), that is, outside the DUPAL anomaly, with the exception of the Samoa Islands. Samoan lavas are a special case; they are characterized by an enrichment in enriched mantle 2 (EM2) component[26] and a deep-mantle tomographic connection[20,27], but they also represent a good example of subduction–plume interaction[28], thus no longer the product of a pristine deep plume. Despite the complexity of Samoa, all basalts from the Pacific mantle domain plot on a mixing line between the prevalent mantle ($PREMA_{W15}$) as defined by White[13], and the depleted MORB mantle (DMM)[13].

By contrast, the majority of basalts from the African mantle domain generally have higher $^{87}Sr/^{86}Sr$ (up to 0.706) and elevated $^{207}Pb/^{204}Pb$ and $^{208}Pb/^{204}Pb$ ratios for a given $^{206}Pb/^{204}Pb$ ratio, lying within the DUPAL anomaly. The African mantle domain thus appears to be a mixture between $PREMA_{W15}$, enriched mantle 1 and 2 source endmembers (EM1 and EM2, respectively) and the DMM. It is therefore characterized by a distinctive enriched component that is not detected in the Pacific mantle domain, which has a more depleted signature. Our results therefore show that heterogeneities in the present-day deep mantle are not controlled by a north–south hemispheric subdivision previously ascribed to the DUPAL anomaly[13,16]. Instead, they are dominantly controlled by the two antipodal mantle domains associated with the two LLSVPs and centred on the equator.

Genesis of the geochemical mantle dichotomy

Seismic tomography demonstrates contrasting geometries for the two LLSVPs, with the African LLSVP being ~30% more voluminous and exhibiting higher topography (that is, height above the core–mantle boundary) than the Pacific LLSVP[1,29]. Collectively, the compositional dichotomy between the two mantle domains, and morphological difference between the two LLSVPs, invites the question of whether (1) the mantle domains (including their LLSVPs) formed in different periods of Earth history and/or (2) they have had distinct evolutionary histories.

Competing models consider LLSVPs either as long-lived structures formed during the very early stages of planetary differentiation[21,30] or as transient features that correspond with the supercontinent cycle through the accumulation of subducted oceanic lithosphere at the core–mantle boundary below an evolving subduction girdle[3]. Proponents of the long-lived LLSVP model[1,2] have used anomalous ratios (compared with the bulk-silicate Earth) of isotopic systems with short half-lives (<100 Myr; for example, $^{182}Hf/^{182}W$ and $^{146}Sm/^{142}Nd$) in OIBs[31,32] to support their argument. The assumption is that rapid radioactive decay would yield only daughter isotopes in the earliest history of the Solar System (≥4,100 Ma), and such isotopes can thus be used to trace primordial mantle reservoirs hidden in the deep mantle. However, more recent work has shown that such anomalous signatures could potentially reflect the ongoing transfer of core material to the lower mantle, triggered by subducted slabs impinging the core–mantle boundary[33], thus rendering the assumption invalid. Even if the assumption were valid, the presence of anomalous short-lived radiogenic isotope ratios cannot unequivocally distinguish between the two contrasting LLSVP models as the dynamic LLSVP model also assumes the presence of a dense and primordial lower mantle layer[3,4]. Indeed, such a feature (or other primordial mantle features) has been reported from a variety of modern plumes, some closely linked to the LLSVPs (for example, at Ontong Java and Réunion[31,32]) and others located away from the LLSVPs[31,34].

Here, we argue that our reported deep-mantle geochemical dichotomy in long-lived isotopes between the African and Pacific

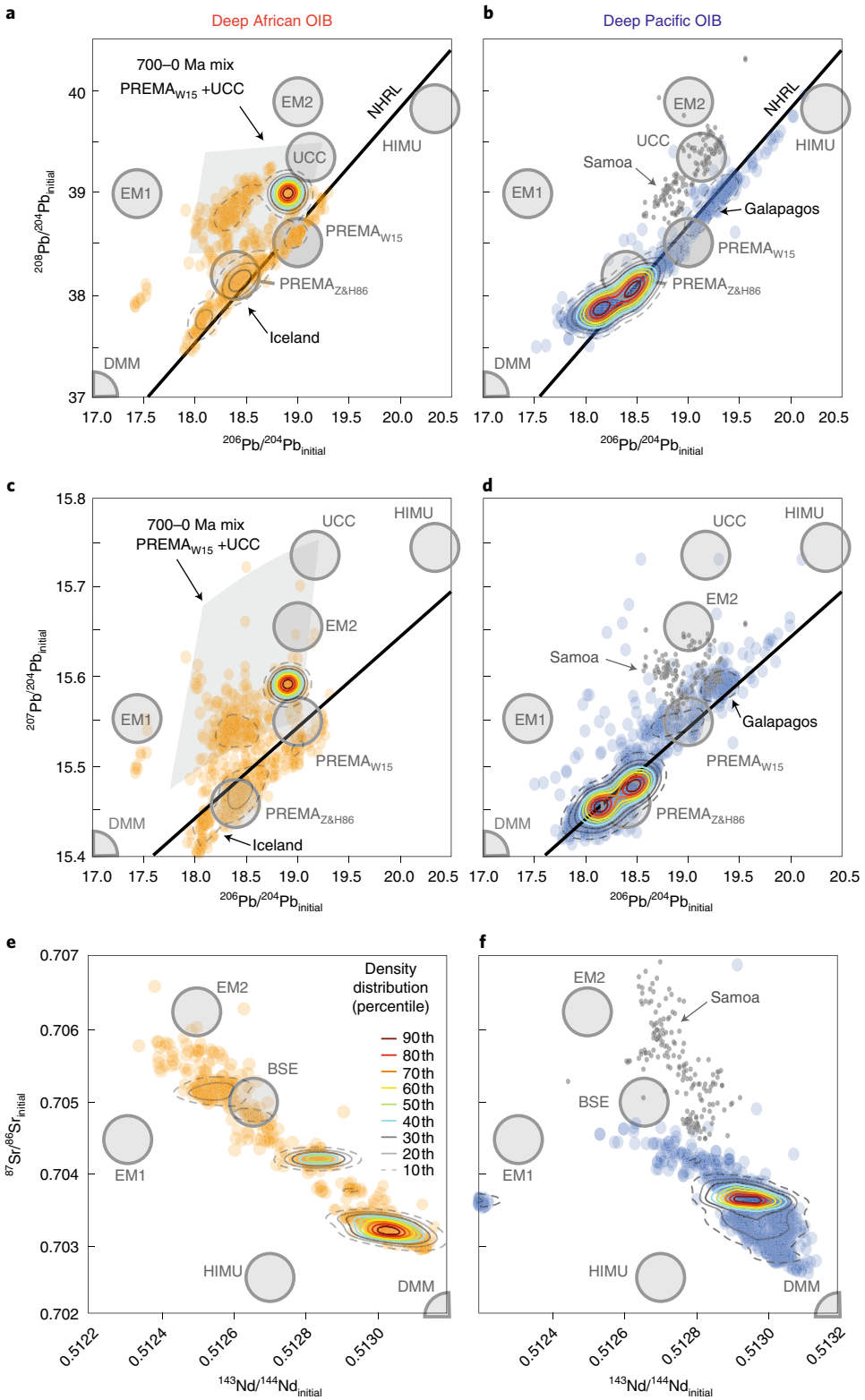

Fig. 2 | Isotopic data of OIBs and OPBs derived from the deep source of the African and the Pacific mantle domains. Isotopic compositions are back-calculated to initial compositions at the time of crystallization for Kerguelen and Ontong Java oceanic plateaus. a,**b**, $^{206}Pb/^{204}Pb$ versus $^{208}Pb/^{204}Pb$. **c**,**d**, $^{206}Pb/^{204}Pb$ versus $^{207}Pb/^{204}Pb$. **e**,**f**, $^{143}Nd/^{144}Nd$ versus $^{87}Sr/^{86}Sr$. The contour lines represent percentiles of the kernel density estimation (see Methods). Also shown are the NHRL[16] that defines the DUPAL anomaly (above the NRHL), the prevalent mantle defined by Zindler and Hart[38] (PREMA$_{Z\&H86}$) and by White[13] (PREMA$_{W15}$), enriched mantle 1 (EM1), enriched mantle 2 (EM2), high-μ (HIMU) and the UCC isotopic endmembers[13]. The grey fields shown in **a** and **c** are mixing modelling results of PREMA$_{W15}$ + UCC between 700 and 0 Ma.

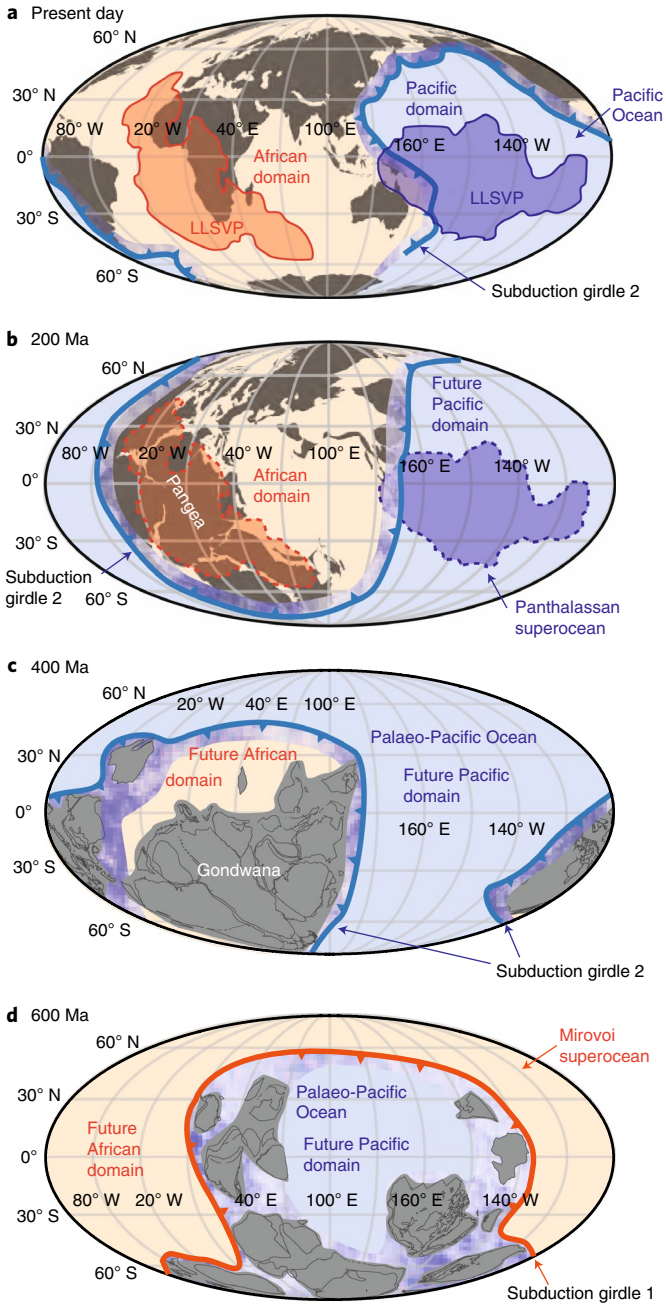

Fig. 3 | Configurations of the continental masses and African and Pacific mantle domains for the present day, 200 Ma, 400 Ma and 600 Ma. **a**, Present-day configuration with positions of the two mantle domains and their respective LLSVPs (orange for the African domain and blue for the Pacific domain) and the circum-Pacific subduction girdle. **b**, Pangaea configuration at 200 Ma[39]. **c**, Pangaea assembly process at 400 Ma[35]. **d**, Rodinia break-up and Gondwana assembly at 600 Ma[35]. Note the contour shapes of the LLSVPs in **b** are speculative and based on their present-day configuration (Fig. 1). The maps are centred on the Equator and 100th meridian, and each meridian is separated by 30°.

mantle domains points to a geochemical 'memory' of mantle domains linked to the supercontinent cycle and related superocean evolution[35]. The composition of the whole mantle has evolved over time through the competing effects of (1) progressive depletion by extraction of mafic magma (that is, through partial melting of mantle peridotite, most commonly along mid-ocean ridges and arcs) and (2) enrichment by recycling of lithosphere and sediments through subduction or crustal delamination[36]. The result is a complex mixture between the prevalent mantle and different mantle components defined as isotopic endmembers—DMM on the one hand (that is, the depleted mantle source of MORBs)[13] and continental crustal material or sediments derived from it (EM1), oceanic crust and marine sediments (EM1) and ancient slab or lithospheric mantle (HIMU) on the other hand—being generally ascribed to assimilation of EM1, EM2 and HIMU[13]. The $PREMA_{W15}$–DMM trend of basalts from the Pacific domain indicates that the chemical characteristics of this mantle domain are controlled chiefly by a pure mantle component (that is, by melt extraction). By contrast, the compositions of the basalts from the African mantle domain lie between $PREMA_{W15}$ and the upper continental crust (UCC)[13], which is consistent with the addition of recycled material into the deep mantle. Accordingly, the dominant process that imparts its isotopic signature in the African domain is the subduction of continental-derived material. The isotopic composition of the source for the African domain OIBs can be modelled by a simple mixing between $PREMA_{W15}$ and continental components (that is, UCC) as old as 700 Ma (Fig. 2a,b and Supplementary Data 3).

The legacy of the supercontinent and superocean cycles

We therefore hypothesize that the deep-mantle dichotomy that distinguishes the two mantle domains as sampled by deep plumes originated from the formation and demise of successive supercontinents and superoceans over the past ~700 Myr. The Pacific mantle domain (Fig. 3a) is proposed to have developed from the breakup of the Neoproterozoic and penultimate supercontinent Rodinia after ~700 Ma—commonly referred to as the Palaeo-Pacific Ocean (Fig. 3d) or the later Panthalassan superocean (Fig. 3b). Due to the switch of subduction polarity from that of subduction girdle 1 directed towards the future Pacific domain (Fig. 3d) to that of subduction girdle 2 directed towards the future African domain soon after the breakup of the supercontinent Rodinia ~600 Ma (Fig. 3a–c)[35], little continental material has been recycled into the Pacific mantle domain. By contrast, the African domain evolved from the Gondwanan (Fig. 3c,d) and Pangaean (Fig. 3b,c) assembly over a slab graveyard through a prolonged subduction and ocean closures (the gradual closure of the Mirovoi superocean; Fig. 3c,d)[35], thus inheriting important subducted continental materials. In addition, continental materials have also been brought down there by subduction girdle 2 (Fig. 3a–c)[35]. Therefore, the African domain exhibits the observed isotopic enrichment towards EM1 and EM2.

Thus, subduction polarity associated with the supercontinent cycle and superocean evolution can best explain why the African mantle domain is contaminated with continental crustal materials, whereas the Pacific mantle domain has been protected from such contamination for much of the past 600 Myr. The deep-mantle geochemical dichotomy therefore shows that the two mantle domains (including the LLSVPs) may have been geodynamically and chemically coupled with the supercontinent cycles, thus suggesting a dynamic, instead of the stationary, nature of the mantle structure and composition.

Online content

Any methods, additional references, Nature Research reporting summaries, source data, extended data, supplementary information, acknowledgements, peer review information; details of author contributions and competing interests; and statements of data and code availability are available at https://doi.org/10.1038/s41561-020-0599-9.

Received: 28 November 2019; Accepted: 22 May 2020;
Published online: 29 June 2020

References

1. Burke, K., Steinberger, B., Torsvik, T. H. & Smethurst, M. A. Plume generation zones at the margins of large low shear velocity provinces on the core–mantle boundary. *Earth Planet. Sci. Lett.* **265**, 49–60 (2008).
2. Dziewonski, A. M., Lekic, V. & Romanowicz, B. A. Mantle anchor structure: an argument for bottom up tectonics. *Earth Planet. Sci. Lett.* **299**, 69–79 (2010).
3. Li, Z.-X. & Zhong, S. Supercontinent–superplume coupling, true polar wander and plume mobility: plate dominance in whole-mantle tectonics. *Phys. Earth Planet. Inter.* **176**, 143–156 (2009).
4. Anderson, D. L. Superplumes or supercontinents? *Geology* **22**, 39–42 (1994).
5. Bunge, H.-P. et al. Time scales and heterogeneous structure in geodynamic Earth models. *Science* **280**, 91–95 (1998).
6. McNamara, A. K. & Zhong, S. Thermochemical structures beneath Africa and the Pacific Ocean. *Nature* **437**, 1136–1139 (2005).
7. Li, Z. X. et al. Assembly, configuration, and break-up history of Rodinia: a synthesis. *Precambrian Res.* **160**, 179–210 (2008).
8. Mitchell, R. N., Kilian, T. M. & Evans, D. A. D. Supercontinent cycles and the calculation of absolute palaeolongitude in deep time. *Nature* **482**, 208–211 (2012).
9. Evans, D. A. True polar wander, a supercontinental legacy. *Earth Planet. Sci. Lett.* **157**, 1–8 (1998).
10. Gamal El Dien, H., Doucet, L. S., Li, Z.-X., Cox, M. C. & Mitchell, R. N. Global geochemical fingerprinting of plume intensity suggests coupling with the supercontinent cycle. *Nat. Commun.* **10**, 5270 (2019).
11. Doucet, L. S. et al. Coupled supercontinent–mantle plume events evidenced by oceanic plume record. *Geology* **48**, 159–163 (2020).
12. Jackson, M. G. et al. Evidence for the survival of the oldest terrestrial mantle reservoir. *Nature* **466**, 853–856 (2010).
13. White, W. M. Isotopes, DUPAL, LLSVPs, and anekantavada. *Chem. Geol.* **419**, 10–28 (2015).
14. Class, C. & Goldstein, S. L. Evolution of helium isotopes in the Earth's mantle. *Nature* **436**, 1107–1112 (2005).
15. Dupré, B. & Allègre, C. J. Pb–Sr isotope variations in Indian Ocean basalts and mixing phenomena. *Nature* **303**, 142–146 (1983).
16. Hart, S. R. A large-scale anomaly in the Southern Hemisphere mantle. *Nature* **309**, 753–757 (1984).
17. Staudigel, H. et al. The longevity of the South Pacific isotopic and thermal anomaly. *Earth Planet. Sci. Lett.* **102**, 24–44 (1991).
18. Castillo, P. The Dupal anomaly as a trace of the upwelling lower mantle. *Nature* **336**, 667–670 (1988).
19. Jackson, M., Becker, T. & Konter, J. Geochemistry and distribution of recycled domains in the mantle inferred from Nd and Pb isotopes in oceanic hot spots: implications for storage in the large low shear wave velocity provinces. *Geochem. Geophys. Geosyst.* **19**, 3496–3519 (2018).
20. French, S. W. & Romanowicz, B. Broad plumes rooted at the base of the Earth's mantle beneath major hotspots. *Nature* **525**, 95–99 (2015).
21. Torsvik, T. H., Steinberger, B., Ashwal, L. D., Doubrovine, P. V. & Trønnes, R. G. Earth evolution and dynamics—a tribute to Kevin Burke. *Can. J. Earth Sci.* **53**, 1073–1087 (2016).
22. Hager, B. H., Clayton, R. W., Richards, M. A., Comer, R. P. & Dziewonski, A. M. Lower mantle heterogeneity, dynamic topography and the geoid. *Nature* **313**, 541–545 (1985).
23. Courtillot, V., Davaille, A., Besse, J. & Stock, J. Three distinct types of hotspots in the Earth's mantle. *Earth Planet Sci. Lett.* **205**, 295–308 (2003).
24. Jackson, M. G., Konter, J. G. & Becker, T. W. Primordial helium entrained by the hottest mantle plumes. *Nature* **542**, 340–343 (2017).
25. Becker, T. W. & Boschi, L. A comparison of tomographic and geodynamic mantle models. *Geochem. Geophys. Geosyst.* **3**, 1003 (2002).
26. Jackson, M. G. et al. The return of subducted continental crust in Samoan lavas. *Nature* **448**, 684–687 (2007).
27. Boschi, L., Becker, T. & Steinberger, B. Mantle plumes: dynamic models and seismic images. *Geochem. Geophys. Geosyst.* **8**, Q10006 (2007).
28. Druken, K., Kincaid, C., Griffiths, R., Stegman, D. & Hart, S. Plume–slab interaction: the Samoa–Tonga system. *Phys. Earth Planet. Inter.* **232**, 1–14 (2014).
29. Cottaar, S. & Lekic, V. Morphology of seismically slow lower-mantle structures. *Geophys. J. Int.* **207**, 1122–1136 (2016).
30. Bebout, G. E., Bebout, A. E. & Graham, C. M. Cycling of B, Li, and LILE (K, Cs, Rb, Ba, Sr) into subduction zones: SIMS evidence from micas in high-P/T metasedimentary rocks. *Chem. Geol.* **239**, 284–304 (2007).
31. Rizo, H. et al. Preservation of Earth-forming events in the tungsten isotopic composition of modern flood basalts. *Science* **352**, 809–812 (2016).
32. Mundl, A. et al. Tungsten-182 heterogeneity in modern ocean island basalts. *Science* **356**, 66–69 (2017).
33. Rizo, H. et al. ^{182}W evidence for core-mantle interaction in the source of mantle plumes. *Geochemical Perspect. Lett.* **11**, 6–11 (2019).
34. Wang, X.-C. et al. Identification of an ancient mantle reservoir and young recycled materials in the source region of a young mantle plume: implications for potential linkages between plume and plate tectonics. *Earth Planet. Sci. Lett.* **377-378**, 248–259 (2013).
35. Li, Z. X. et al. Decoding Earth's rhythms: modulation of supercontinent cycles by longer superocean episodes. *Precambrian Res.* **323**, 1–5 (2019).
36. Willbold, M. & Stracke, A. Formation of enriched mantle components by recycling of upper and lower continental crust. *Chem. Geol.* **276**, 188–197 (2010).
37. Doubrovine, P. V., Steinberger, B. & Torsvik, T. H. A failure to reject: testing the correlation between large igneous provinces and deep mantle structures with EDF statistics. *Geochem. Geophys. Geosyst.* **17**, 1130–1163 (2016).
38. Zindler, A. & Hart, S. Chemical geodynamics. *Annu. Rev. Earth Planet Sci.* **14**, 493–571 (1986).
39. Matthews, K. J. et al. Global plate boundary evolution and kinematics since the late Paleozoic. *Glob. Planet. Change* **146**, 226–250 (2016).

Methods

Radiogenic isotopic data. All the Pb, Nd and Sr isotopic data used in this study are available from the Earthchem Portal (www.earthchem.org). Precompiled datasets are available on GEOROC (http://georoc.mpch-mainz.gwdg.de/georoc/) for each ocean island and oceanic plateau used in this study. We downloaded the isotopic data for 16 OIBs and 2 oceanic large igneous provinces in July 2019 (Fig. 1). From the entire datasets, we selected the sample with basaltic affinities (SiO_2 from 40 to 55 wt.% and $Na_2O + K_2O$ below 10 wt.%)[40] for which Pb, Nd and Sr isotopic data are available. A total of ~6,030 samples were filtered from the online database; the isotopic data, together with sample coordinates, are reported in Supplementary Data 1 for the African domain and in Supplementary Data 2 for the Pacific domain.

From these initial datasets, we filtered the deep-source hotspots and oceanic plateau from hotspots and oceanic plateau with ambiguous source (see criteria in the following). We also excluded data where continental crustal or lithospheric contamination were previously reported (for example, Kerguelen basalt older than 95 Ma)[41]. The filtered datasets contain 2,608 samples covering 4 ocean islands and 2 oceanic plateaus of deep-plume origin (Supplementary Data 1 and 2).

Because we compare present-day OIBs with those of oceanic plateaus up to 125 Ma, we applied an age correction to compute the initial isotopic data at the time of basalt crystallization for samples from the Kerguelen and Ontong Java plateaus (Supplementary Data 1 and 2). Such a calculation requires the consideration of elemental abundances, specifically those of uranium (U), thorium (Th) and Pb for $^{206}Pb/^{204}Pb$, $^{207}Pb/^{204}Pb$ and $^{208}Pb/^{204}Pb$, samarium (Sm) and Nd for $^{144}Nd/^{143}Nd$, and rubidium (Rb) and Sr for $^{87}Sr/^{86}Sr$ age corrections. The age-corrected isotopic data are presented in Fig. 2. In Fig. 2 and Extended Data Fig. 1, we used bivariate kernel density estimation[42] modified by ref. [43]. Both the Matlab script and the dataset used for generating the figures are given in Supplementary Data 4.

Radiogenic isotopic mixing. We model the Pb isotopic composition of sediments with UCC composition and PREMA for the past 700 Myr. For sediments with UCC composition, we use present-day values of $^{206}Pb/^{204}Pb = 19.25$, $^{207}Pb/^{204}Pb = 15.75$ and $^{238}U/^{204}Pb = 9.74$[44], and for $PREMA_{W15}$, we use $^{206}Pb/^{204}Pb = 19$, $^{207}Pb/^{204}Pb = 15.55$ and $^{238}U/^{204}Pb = 8.6$[13]. The equation and the calculation are presented in Supplementary Data 3.

Tomography used in Fig. 1. For the seismically imaged lower-mantle thermochemical structures, we adopt here the s5mean model of Doubrovine et al.[37] that is stacked from five shear-wave models: GyPSuM of Simmons et al.[45], HMSL-S of Houser et al.[46], S40RTS of Ritsema et al.[47], S362ANI of Kustowski et al.[48] and SAW642AN of Megnin and Romanowicz[49]. Velocity perturbations at the 2,800-km slice represent averages of those velocities from each of the input models after the removal of layer mean velocities of Doubrovine et al.[37].

Deep-mantle plume data and selection criteria. All the isotopic data are extracted from the Earthchem portal, and for each hotspot and oceanic plateau these data can be downloaded at https://www.earthchem.org/. The primary selection criteria are (1) flood basalts in the early history of the plume activity[23], (2) long-lived hotspots track[23], (3) unambiguous tomographic evidence for plume tails down to the core–mantle boundary[20,25] and (4) high $(^3He/^4He)_{sample}$ / $(^3He/^4He)_{atmosphere}$ (R/R_A) ratios, where ratio $R/R_A > 10$ (that is, 10 times above MORB[24]). We apply the criteria to a list of hotspots and oceanic plateaus from above the African and Pacific LLSVPs. Each hotspot is given a score from 0 to 4 according to the number of criteria it meets. Each missing criterion is marked as a '+' on the final grade as a benefit of doubt. Hotspots with a total of 4 or 3+ are considered to be derived from a deep-mantle source. In the following, we review all criteria for plumes arising from the African and Pacific LLSVPs. Among modern oceanic plateaus and hotspots associated with the African and Pacific mantle domains, eight hotspots score 4 or 3+: Tristan da Cunha, Réunion, Iceland and Kerguelen Plateau for the African mantle domain and Hawaii, Easter Islands, Galapagos and Ontong Java for the Pacific mantle domain.

Deep-sourced hotspots and oceanic plateau. The Tristan da Cunha (3) hotspots are a series of hotspot tracks[50] that are believed to have commenced ~132 Ma[27] with the production of the Paraná–Etendeka Traps followed by the Walvis Ridge hotspot track[51–53]. The deep source for the Tristan plume is detected by all three tomography catalogues[20,27]. The helium isotopic ratio ($^3He/^4He$) of Tristan basalts has a maximum R/R_A value of ~7 and is below the R/R_A threshold of 10. However, the low R/R_A can be explained by shallow-level mixing of the deep source by more evolved upper-mantle material causing degassing[54], Tristan da Cunha has been classified among the deep-sourced primary plume by previous studies[23], and on the basis of the $^3He/^4He$ ambiguity, we define the He isotopic signal as + for Tristan de Cunha.

The Kerguelen (4) oceanic plateau formed 120 to 95 Ma[55] and was followed by the long-lived Ninetyeast Ridge (>82 Ma to 37 Ma) hotspot track and Broken Ridge plateau (95 Ma)[53,55]. The Kerguelen plume is suspected to be still active with recent volcanic activity in the Kerguelen Archipelago and Heard Island[55]. The deep source for the Kerguelen plume is detected by all three tomography catalogues[20,27]. Basalts from Kerguelen archipelago exhibit R/R_A more than 10 times higher than MORB[56]. The recently published compilation of Olierook et al.[41] indicates that pre-95 Ma Kerguelen basalts are contaminated by lithospheric mantle during emplacement and do not solely represent the deep-mantle source. Therefore, we select only the post-95 Ma basalts.

The Réunion (4) plume track starts with the buildup of the Deccan Traps (ca. 66 Ma)[53] and the formation of a subsequent long-lived hotspot track[57] still active today. The deep source of the Réunion plume is detected by all three tomographic catalogues[20,27]. Basalts from the Réunion island have R/R_A 10 times higher than MORB[58].

The Easter (4) plume started with the building of the mid-Pacific seamount flood basalts and produced a hotspot track that is still active today with Easter Island and associated seamounts[53]. The deep source of the Easter plume is detected by all three tomography catalogues[20,27]. Basalts from the Easter microplate and Easter seamount exhibit an $R/R_A \geq 10$ times that of the atmosphere[59,60].

The Hawaii (3) plume might have started with flood basalts or a large igneous provinces that is now subducted[61], and it is followed by the Emperor and Hawaii chains[53]. The deep source of the Hawaii plume is detected by all three tomography catalogues[20,27]. Basalts from Hawaii exhibit high $R/R_A > 10$ times that of the atmosphere[62,63].

The Louisville/Ontong Java Plateau (4): the Louisville hotspot started around 125 Ma with the build-up of the Ontong Java Plateau followed by a hotspot track still active today[53,64]. The deep source of the Louisville plume is detected by all three tomography catalogues[20,27]. Basalts from Louisville exhibit high R/R_A above 10 time that of the atmosphere[62,63].

The Iceland (4) plume may have produced the North Atlantic Volcanic Province[65,66] and a non-conventional oceanic hotspot track[67] because Iceland is located on a mid-ocean ridge. A deep source for the Iceland plume is suggested by all three tomography catalogues[20,27], and Iceland basalts display high R/R_A above 10 time that of the atmosphere[54]. However, it is important to note that the plume origin of the North Atlantic Volcanic Province is questioned by some[67], in that the Iceland plume might have predated its emplacement, and the North Atlantic Volcanic Province may thus reflect rifting in the vicinity of existing thinned crust instead of the arrival of a plume head. Moreover, a recent isotopic study suggests that some Iceland lavas were contaminated by continental materials[68].

The Galapagos (3) plume started with the Caribbean large igneous province and produced a hotspot track[69]. A deep origin of the plume is detected by only one tomographic catalogue[20]. Basalts from the Galapagos hotspots exhibit R/R_A more than 10 times that of the atmosphere[70,71].

Hotspots and oceanic plateaus with ambiguous sources. Although St Helena (1) island did not start with flood basalt or as a large igneous province, in its early stages it exhibited a hotspot track that started probably at ca. 80 Ma[23,53]. However, the St Helena track, in contrast with other hotspots tracks, is not well defined and corresponds to broad and ill-defined scattered seamounts and volcanic ridges[72]. The basalts from St Helena display low $R/R_A < 5$[73]. The St Helena plume is detected by all three tomography catalogues[20,27]. The absence of flood basalt in the early history of the St Helena plume, the ill-defined track and the low R/R_A do not support a deep primary origin.

The Azores, Comoros, Cape Verde and Madeira/Canary (0–2) hotspots did not start with a flood basalt or large igneous provinces and are not characterized by a hotspot track[53,74,75]. The Azores, Comoros and Cape Verde plumes are detected by only one tomography catalogue[20], and the Madeira/Canary hotspot is detected by only two catalogues[20,27]. Basalts from Azores exhibit high R/R_A more than 10 times that of the atmosphere[76]. Basalts from Comores, Cape Verde and Madeira/Canary exhibit low R/R_A[14,77,78]. Isotopic composition of the Cape Verde basalts appears to reflect lithospheric contaminations[77].

The Marquesas (2) plume started with the Shatsky Rise but did not produce hotspot tracks[53,79] and is detected by only one catalogue[20]. Basalts from the Marquesas hotspot exhibit R/R_A more than 10 times that of the atmosphere[70,80].

The Society, Samoa, Pitcairn and Cook–Austral islands (2) hotspots did not start with large igneous provinces and are not characterized by a hotspot track[53]. The Society and Samoa plumes are detected by two catalogues[20,27] while the Pitcairn and Cook–Austral plumes are only detected by one catalogue[20]. The basalts from the Society, Samoa, Pitcairn and Cook–Austral islands hotspots exhibit R/R_A more than 10 times that of the atmosphere[81–83]. Samoa is a special case and has been characterized as a good example of slab and plume interaction[28].

Data availability

The data supporting the findings of this study are available on the Georoc database (http://georoc.mpch-mainz.gwdg.de/georoc/).

Code availability

The Matlab files used for statistical distribution of the isotopic data are available from the corresponding author upon request.

References

40. Le Bas, M. IUGS reclassification of the high-Mg and picritic volcanic rocks. *J. Petrol.* **41**, 1467–1470 (2000).

41. Olierook, H. K., Jiang, Q., Jourdan, F. & Chiaradia, M. Greater Kerguelen large igneous province reveals no role for Kerguelen mantle plume in the continental breakup of eastern Gondwana. *Earth Planet. Sci. Lett.* **511**, 244–255 (2019).
42. Botev, Z. I., Grotowski, J. F. & Kroese, D. P. Kernel density estimation via diffusion. *Ann. Stat.* **38**, 2916–2957 (2010).
43. Spencer, C. J. et al. Deconvolving the pre-Himalayan Indian margin—tales of crustal growth and destruction. *Geosci. Front.* **10**, 863–872 (2019).
44. Asmerom, Y. & Jacobsen, S. B. The Pb isotopic evolution of the Earth: inferences from river water suspended loads. *Earth Planet. Sci. Lett.* **115**, 245–256 (1993).
45. Simmons, N. A., Forte, A. M., Boschi, L. & Grand, S. P. GyPSuM: a joint tomographic model of mantle density and seismic wave speeds. *J. Geophys. Res. Solid Earth* **115** (2010).
46. Houser, C., Masters, G., Shearer, P. & Laske, G. Shear and compressional velocity models of the mantle from cluster analysis of long-period waveforms. *Geophys. J. Int.* **174**, 195–212 (2008).
47. Ritsema, J., Deuss, A. A., Van Heijst, H. & Woodhouse, J. S40RTS: a degree-40 shear-velocity model for the mantle from new Rayleigh wave dispersion, teleseismic traveltime and normal-mode splitting function measurements. *Geophys. J. Int.* **184**, 1223–1236 (2011).
48. Kustowski, B., Ekström, G. & Dziewoński, A. Anisotropic shear-wave velocity structure of the Earth's mantle: a global model. *J. Geophys. Res. Solid Earth* **113** (2008).
49. Mégnin, C. & Romanowicz, B. The three-dimensional shear velocity structure of the mantle from the inversion of body, surface and higher-mode waveforms. *Geophys. J. Int.* **143**, 709–728 (2000).
50. Müller, R. D., Royer, J.-Y. & Lawver, L. A. Revised plate motions relative to the hotspots from combined Atlantic and Indian Ocean hotspot tracks. *Geology* **21**, 275–278 (1993).
51. Gibson, S., Thompson, R. & Day, J. Timescales and mechanisms of plume–lithosphere interactions: $^{40}Ar/^{39}Ar$ geochronology and geochemistry of alkaline igneous rocks from the Paraná–Etendeka large igneous province. *Earth Planet. Sci. Lett.* **251**, 1–17 (2006).
52. Gibson, S., Thompson, R., Leonardos, O., Dickin, A. & Mitchell, J. The limited extent of plume–lithosphere interactions during continental flood-basalt genesis: geochemical evidence from Cretaceous magmatism in southern Brazil. *Contrib. Mineral. Petrol.* **137**, 147–169 (1999).
53. Johansson, L., Zahirovic, S. & Müller, R. D. The interplay between the eruption and weathering of large igneous provinces and the deep-time carbon cycle. *Geophys. Res. Lett.* **45**, 5380–5389 (2018).
54. Hilton, D., Barling, J. & Wheller, G. Effect of shallow-level contamination on the helium isotope systematics of ocean-island lavas. *Nature* **373**, 330–333 (1995).
55. Coffin, M. F. et al. Kerguelen hotspot magma output since 130 Ma. *J. Petrol.* **43**, 1121–1137 (2002).
56. Doucet, S. et al. Primitive neon and helium isotopic compositions of high-MgO basalts from the Kerguelen Archipelago, Indian Ocean. *Earth Planet Sci. Lett.* **241**, 65–79 (2006).
57. Storey, B. C. The role of mantle plumes in continental breakup: case histories from Gondwanaland. *Nature* **377**, 301–308 (1995).
58. Graham, D., Lupton, J., Albarède, F. & Condomines, M. Extreme temporal homogeneity of helium isotopes at Piton de la Fournaise, Réunion Island. *Nature* **347**, 545–548 (1990).
59. Stroncik, N., Niedermann, S., Schnabel, E. & Erzinger, J. Determining the geochemical structure of the mantle from surface isotope distribution patterns? Insights from Ne and He isotopes and abundance ratios. *AGU Fall Meeting 2011* abstr. V51B-2519 (AGU, 2011).
60. Poreda, R., Schilling, J.-G. & Craig, H. Helium isotope ratios in Easter microplate basalts. *Earth Planet. Sci. Lett.* **119**, 319–329 (1993).
61. Head, J. W. & Coffin, M. F. in *Large Igneous Provinces: Continental, Oceanic, and Planetary Flood Volcanism* (eds Mahoney, J. J. & Coffin, M. F.) 411–438 (AGU, 1997).
62. Kurz, M. D., Jenkins, W. J., Hart, S. R. & Clague, D. Helium isotopic variations in volcanic rocks from Loihi Seamount and the Island of Hawaii. *Earth Planet. Sci. Lett.* **66**, 388–406 (1983).
63. Kurz, M., Jenkins, W. & Hart, S. Helium isotopic systematics of oceanic islands and mantle heterogeneity. *Nature* **297**, 43–47 (1982).
64. Olierook, H. K., Jourdan, F. & Merle, R. E. Age of the Barremian–Aptian boundary and onset of the Cretaceous Normal Superchron. *Earth Sci. Rev.* **197**, 102906 (2019).
65. Graham, D. W. et al. Helium isotope composition of the early Iceland mantle plume inferred from the Tertiary picrites of West Greenland. *Earth Planet Sci. Lett.* **160**, 241–255 (1998).
66. Storey, M., Duncan, R. A. & Tegner, C. Timing and duration of volcanism in the North Atlantic Igneous Province: implications for geodynamics and links to the Iceland hotspot. *Chem. Geol.* **241**, 264–281 (2007).
67. Lawver, L. A. & Müller, R. D. Iceland hotspot track. *Geology* **22**, 311–314 (1994).
68. Torsvik, T. H. et al. Continental crust beneath southeast Iceland. *Proc. Natl Acad. Sci. USA* **112**, E1818–E1827 (2015).
69. Werner, R. et al. Drowned 14-my-old Galápagos archipelago off the coast of Costa Rica: implications for tectonic and evolutionary models. *Geology* **27**, 499–502 (1999).
70. Jackson, M. G., Kurz, M. D. & Hart, S. R. Helium and neon isotopes in phenocrysts from Samoan lavas: evidence for heterogeneity in the terrestrial high $^{3}He/^{4}He$ mantle. *Earth Planet. Sci. Lett.* **287**, 519–528 (2009).
71. Hoernle, K. et al. Existence of complex spatial zonation in the Galápagos plume. *Geology* **28**, 435–438 (2000).
72. Adam, C., Vidal, V. & Escartín, J. 80-Myr history of buoyancy and volcanic fluxes along the trails of the Walvis and St. Helena hotspots (South Atlantic). *Earth Planet. Sci. Lett.* **261**, 432–442 (2007).
73. Graham, D. W., Humphris, S. E., Jenkins, W. J. & Kurz, M. D. Helium isotope geochemistry of some volcanic rocks from Saint Helena. *Earth Planet. Sci. Lett.* **110**, 121–131 (1992).
74. Merle, R. E., Jourdan, F., Chiaradia, M., Olierook, H. K. & Manatschal, G. Origin of widespread Cretaceous alkaline magmatism in the Central Atlantic: a single melting anomaly? *Lithos* **342**, 480–498 (2019).
75. Geldmacher, J., Hoernle, K., van den Bogaard, P., Duggen, S. & Werner, R. New age and geochemical data from seamounts in the Canary and Madeira volcanic provinces: a contribution to the "Great Plume Debate". *AGU Fall Meeting 2004* abstr. V51B 0562 (AGU, 2004).
76. Moreira, M., Doucelance, R., Kurz, M. D., Dupré, B. & Allègre, C. J. Helium and lead isotope geochemistry of the Azores Archipelago. *Earth Planet. Sci. Lett.* **169**, 189–205 (1999).
77. Doucelance, R., Escrig, S., Moreira, M., Gariepy, C. & Kurz, M. D. Pb–Sr–He isotope and trace element geochemistry of the Cape Verde Archipelago. *Geochim. Cosmochim. Acta* **67**, 3717–3733 (2003).
78. Day, J. M. & Hilton, D. R. Origin of $^{3}He/^{4}He$ ratios in HIMU-type basalts constrained from Canary Island lavas. *Earth Planet. Sci. Lett.* **305**, 226–234 (2011).
79. Clouard, V. & Bonneville, A. How many Pacific hotspots are fed by deep-mantle plumes? *Geology* **29**, 695–698 (2001).
80. Castillo, P., Scarsi, P. & Craig, H. He, Sr, Nd, and Pb isotopic constraints on the origin of the Marquesas and other linear volcanic chains. *Chem. Geol.* **240**, 205–221 (2007).
81. Hanyu, T. & Kaneoka, I. The uniform and low $^{3}He/^{4}He$ ratios of HIMU basalts as evidence for their origin as recycled materials. *Nature* **390**, 273–276 (1997).
82. Garapić, G. et al. A radiogenic isotopic (He–Sr–Nd–Pb–Os) study of lavas from the Pitcairn hotspot: implications for the origin of EM-1 (enriched mantle 1). *Lithos* **228**, 1–11 (2015).
83. Moreira, M. & Allègre, C. Helium isotopes on the Macdonald seamount (Austral chain): constraints on the origin of the superswell. *C. R. Geosci.* **336**, 983–990 (2004).

Acknowledgements

This work was supported by the Australian Research Council Laureate Fellowship grant to Z.-X.L. (FL150100133). This is a contribution to IGCP 648. We thank N. Flament and R. Carlson for their constructive comments on earlier versions of the manuscript.

Author contributions

All authors helped with the writing and editing of the manuscript. L.S.D., the primary author, is the main contributor who designed the study, collected the data and drafted the paper. Z.-X.L. conceptualized the initial idea, clarified the relevant concepts, helped to design Fig. 3 and worked with L.S.D. on the writing of the paper. H.G. helped to design the data selection criteria and filtered the database. A.P. helped with the design of the selection criteria. J.B.M. helped to clarify the concepts and validated the approach. W.J.C. provided constraints on the timing of crustal contamination during the assembly of Pangea. N.M. helped with the interpretation of the isotopic compositions of both the African and Pacific domain basalts. H.K.H.O. helped with the data filtering of the Kerguelen samples and the grading of the hotspots and oceanic plateaus. C.J.S. designed the Matlab scripts and performed the statitiscal analysis. R.N.M. helped to clarify some of the concepts.

Competing interests

The authors declare no competing interests.

Additional information

Extended data is available for this paper at https://doi.org/10.1038/s41561-020-0599-9.

Supplementary information is available for this paper at https://doi.org/10.1038/s41561-020-0599-9.

Correspondence and requests for materials should be addressed to L.S.D.

Peer review information Primary Handling Editor: Rebecca Neely.

Reprints and permissions information is available at www.nature.com/reprints.

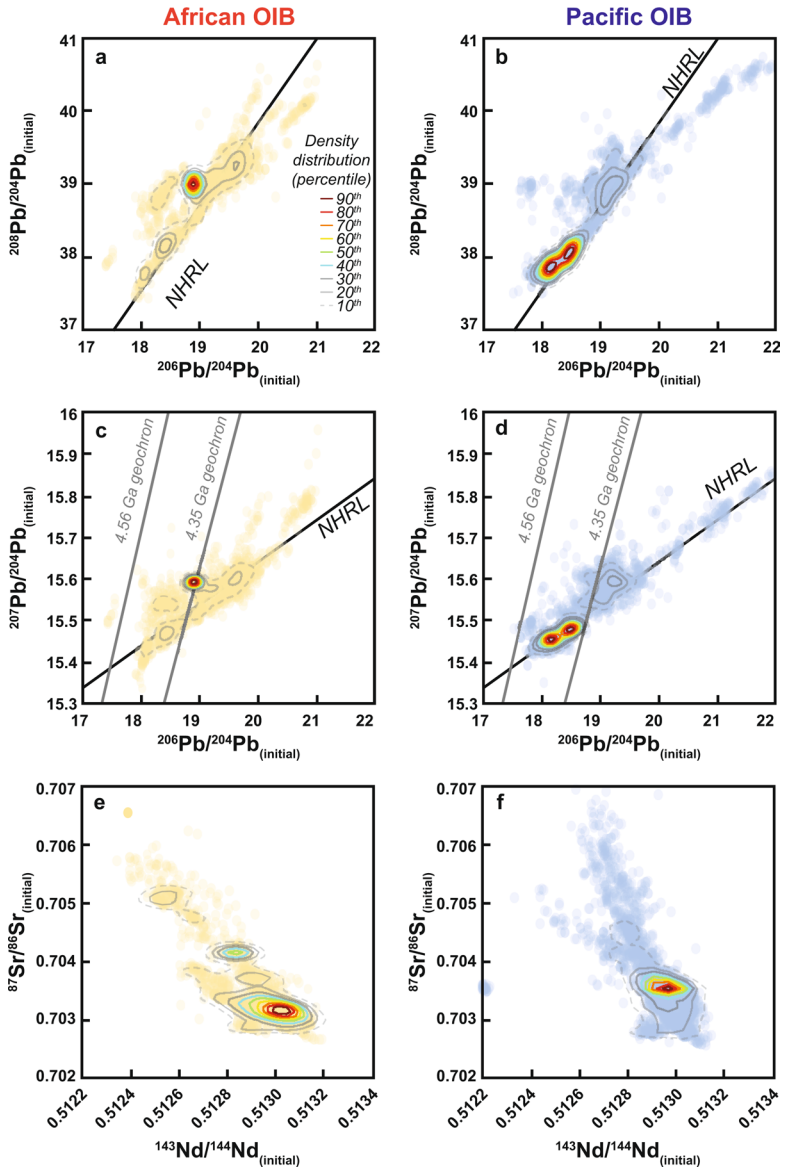

Extended Data Fig. 1 | Isotopic data of Oceanic Island Basalts (OIBs) and Oceanic Plateau Basalts (OPBs) for the African (orange) and the Pacific (blue) mantle domains. The isotope compositions are back-calculated to initial compositions at the time of crystallization for Kerguelen and Ontong Java oceanic plateau basalts. (**a**, **b**) $^{206}Pb/^{204}Pb$ vs. $^{208}Pb/^{204}Pb$ vs. (**c**, **d**) $^{207}Pb/^{204}Pb$ vs. $^{206}Pb/^{204}Pb$, and (**e**, **f**) $^{143}Nd/^{144}Nd$ vs. $^{87}Sr/^{86}Sr$. The contour lines represent percentiles of the kernel density estimation (see Methods). Also shown is the Northern Hemisphere Reference Line (NHRL)[16] that defines the DUPAL anomaly (above the NHRL).

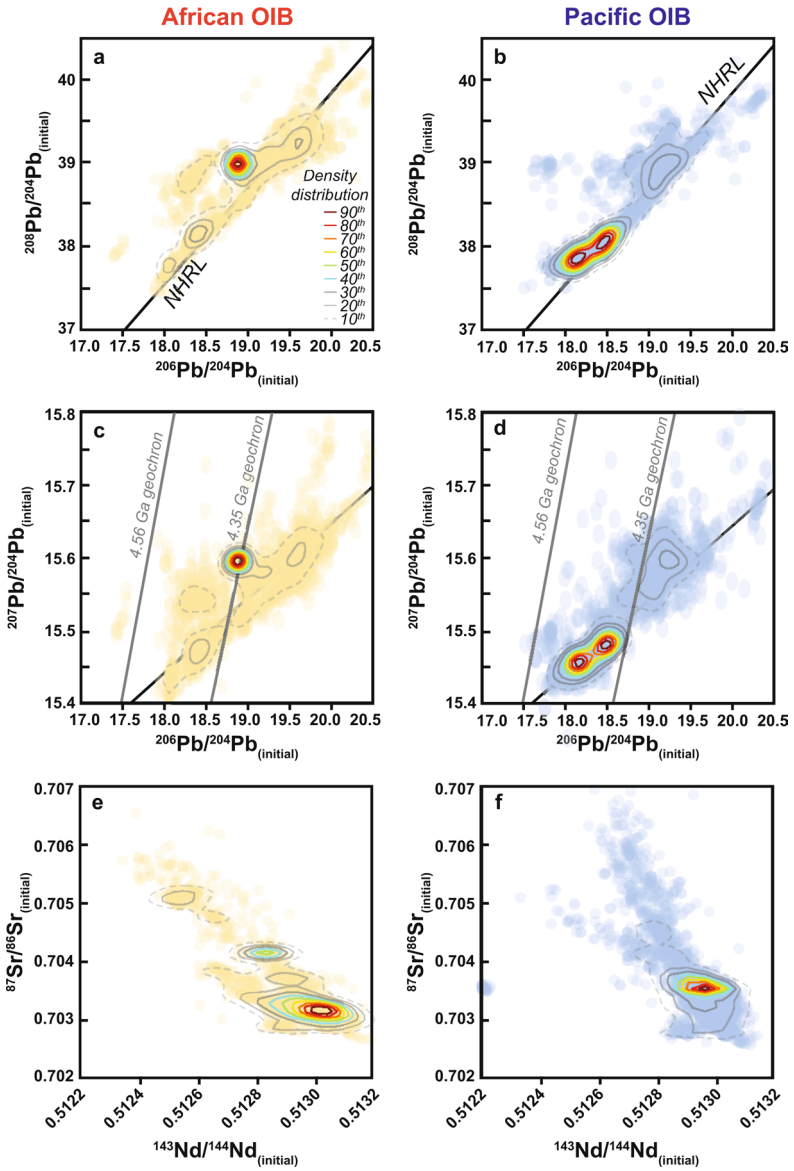

Extended Data Fig. 2 | Isotopic data of Oceanic Island Basalts (OIBs) and Oceanic Plateau Basalts (OPBs) for the African (orange) and the Pacific (blue) mantle Domains, axis scales similar to Fig. 2. The isotope compositions are back-calculated to initial compositions at the time of crystallization for Kerguelen and Ontong Java oceanic plateau basalts. (**a**, **b**) $^{206}Pb/^{204}Pb$ vs. $^{208}Pb/^{204}Pb$ vs. (**c**, **d**) $^{207}Pb/^{204}Pb$ vs. $^{206}Pb/^{204}Pb$, and (**e**, **f**) $^{143}Nd/^{144}Nd$ vs.$^{87}Sr/^{86}Sr$. The contour lines represent percentiles of the kernel density estimation (see Methods). Also shown is the Northern Hemisphere Reference Line (NHRL)[16] that defines the DUPAL anomaly (above the NHRL).

	Flood basalt in early history	Long-lived hotspot track	Tomographic evidence	Max R/R_A		Grading: Courtillot et al. (2003)	Grading: Updated in this study
AFRICAN MANTLE DOMAIN							
La Reunion[P]	**Yes (*Deccan*)**	**Yes**	**Yes**	**14**	**high**	**4**	**4**
Kerguelen(+Heard)[P]	**Yes (*Kerguelen*)**	**Yes**	**Yes**	**18**	**high**	**2+**	**4**
Iceland[P]	**Yes *(NAVP)*?**	**Yes**	**Yes**	**50**	**high**	**4+**	**4**
Tristan[P]	**Yes (*Parana and Edenka*)**	**Yes**	**Yes**	**7.0**	**low**	**3**	**3**
St Helena	No	Yes	No	6.0	low	1	1
Azores	No	No	No	18	high	1+	1
Comores	No	No	No	7.1	low	0+	0
Cape Verde	No	No	No	16	high	2	1
Madeira/Canary	No	No	yes	10	low	2	1
PACIFIC MANTLE DOMAIN							
Easter[P]	**Yes (*mid-pacific seamount*)**	**Yes**	**Yes**	**26***	**high**	**4+**	**4**
Louiseville/Ontong Java[P]	**Yes (*Ontong Java*)**	**Yes**	**Yes**	**11**	**high**	**3+**	**4**
Hawaii[P]	**Subudcted?**	**Yes**	**Yes**	**35**	**high**	**4+**	**3**
Galapagos	**Yes (*Carribean LIP*)**	**Yes**	**No**	**30**	**high**	**2+**	**3**
*Samoa***	*No*	*No*	*Yes*	*34*	high	*4*	*2*
Marquise	Yes (Shatsky)	?	No	14	high	2+	2
Tahiti/Societies	No	No	No	17	high	2+	2
Pitcairn	No	No	No	13	high	2+	2
Cook-Austral	No	No	No	16	high	2+	2

Max R/R_A, higher $(^3He/^4He)_{sample}$ / $(^3He/^4He)_{atmosphere}$

All reference are in the method section

[P], primary deep plume from Courtillot et al. (2003)

*AGU abstract

**Samoa is characterise by plume/subduction interaction

?, the North Atlantic Volcanic Province (NAVP) could reflect rifting in the vicinity of existing thinned crust rather than the arrival of the plume head (Lawver and Muller, 1994).

Extended Data Fig. 3 | List of deep sourced vs. shallower sourced ocean islands and oceanic plateaus from the African and Pacific mantle domain. Scores for the eighteen major OIBs and OPBs with respect to the four criteria are used to determine their deep vs. shallow origins. For details see Methods.